frontiers | Frontiers in Marine Science

TYPE Original Research
PUBLISHED 19 December 2024
DOI 10.3389/fmars.2024.1489943

OPEN ACCESS

EDITED BY
Francisco Javier González,
Instituto Geológico y Minero de España (IGME), Spain

REVIEWED BY
Egidio Marino,
Instituto Geológico y Minero de España (IGME), Spain
Jiangbo Ren,
Guangzhou Marine Geological Survey, China

*CORRESPONDENCE
Xiangwen Ren
renxiangwen@163.com

RECEIVED 02 September 2024
ACCEPTED 28 November 2024
PUBLISHED 19 December 2024

CITATION
Ren X, Hein JR, Yang Z, Xing N and Zhu A (2024) Controls on cobalt concentrations in ferromanganese crusts from the Magellan seamounts, west Pacific. *Front. Mar. Sci.* 11:1489943. doi: 10.3389/fmars.2024.1489943

Controls on cobalt concentrations in ferromanganese crusts from the Magellan seamounts, west Pacific

Xiangwen Ren[1,2]*, James R. Hein[3], Zanzhong Yang[4], Na Xing[5] and Aimei Zhu[1]

[1]Key Laboratory of Marine Geology and Metallogeny, First Institute of Oceanography, Ministry of Natural Resources, Qingdao, China, [2]Laboratory for Marine Geology, Laoshan Laboratory, Qingdao, China, [3]Retired, Soquel, CA, United States, [4]School of Materials Science and Engineering, Shandong University of Technology, Zibo, Shandong, China, [5]Lab of Isotope Marine Chemistry, Xiamen University, Xiamen, Fujian, China

Introduction: Cobalt is the most important critical element in ferromanganese crusts. Co concentration in the Fe-Mn crusts is one of the key parameters for determination of the Co resource. Thus, it is essential to clarify the controls on the variations of Co concentration of ferromanganese crusts.

Methods: To clarify the controls on Co concentration of hydrogenetic nonphosphatized ferromanganese crusts, an equation was deduced based on Fick's First Law: $Co(\%) = Mn0_2(\%) \cdot D_{sw} \cdot \frac{C_{sw}}{\delta} \cdot \frac{z}{GR} \cdot S_{sp}$, and eight potential controls were gleaned from this equation, including dilution, diffusivity of Co ions in seawater (D_{sw}), temperature which controls the D_{sw}, Co ion concentration in seawater (C_{sw}), the diffusion distance of Co ions near the interface of seawater and Fe-Mn crusts (δ), thickness of one molecular layer (z), growth rate (GR), and specific surface area of Fe-Mn crusts (S_{sp}). To constrain the value of Co ion diffusion gradients ($\overline{C_{sw}}/\delta$) and consequently verify the proposed equation, we determined the Co concentrations, growth rates, and specific surface area of the outermost layer of Fe-Mn crusts, and calculated diffusivity of Co^{2+}.

Results: The $\overline{C_{sw}}/\delta$ for the Fe-Mn crusts from Caiwei seamount (Magellan seamounts) was determined to be 295-496 pM/mm, which are reasonable for the Co ion concentrations and seawater mixing in the deep ocean.

Discussion: According to the equation established in this study, the trend of decreasing Co concentrations in Fe-Mn crusts with increasing water depth is controlled mainly by dilution and to a lesser extent by seawater Co ion concentration, temperature of seawater, and consequently the diffusivity of Co ions in seawater.

KEYWORDS

ferromanganese crusts, Magellan seamounts, cobalt, diffusivity, Pacific

1 Introduction

Cobalt (Co) is the most important critical element in ferromanganese crusts (Fe-Mn crusts) due to the high concentrations, economic value, and application in the manufacture of hybrid and electric car batteries, storage of solar energy, magnetic recording media, high-T super-alloys, supermagnets, and smart phones (Hein et al., 2013). Relative to 2020, it's estimated by the International Energy Agency that a 21-fold Co supply will be needed by 2040 to achieve the clean energy transition (IEA, 2021). Compared to the land-based reserve of Co, 11 million tons (U. S. Geological Survey, 2024), the tonnage of in place Co in Fe-Mn crusts from the Pacific Prime Crust Zone (PPCZ) is as high as 50 million tons (Hein and Koschinsky, 2014). Land-based Co ores mainly occur in the West African copper belt (D.R. Congo), with a reserve of 6 million tons, which is 55% of the land-based Co reserves (U. S. Geological Survey, 2024). The average grade of the Co ores in the West African copper belt is 0.12% (Milesi et al., 2006). In contrast, the average Co concentration in Fe-Mn crusts in PPCZ is 0.67% (Hein et al., 2013). Although the mining of Fe-Mn crusts is not currently feasible for technological and economic reasons, Fe-Mn crusts are promising future Co ores.

For determination of the Co resource both before and during mining, Co concentration (grade) in the Fe-Mn crusts is one of the key parameters. However, the Co concentrations in Fe-Mn crusts show regional, local, and stratigraphic (depth in the crusts) variations. The average Co concentrations of Fe-Mn crusts from the seamounts in the Pacific range from 0.3% to 0.8% (Hein et al., 2000). Cobalt concentrations of Fe-Mn crusts show a negative correlation with water depth (Cronan, 1977; Halbach et al., 1983; Manheim, 1986; Andreev and Gramberg, 2002; Benites et al., 2023), and the data show a wide range of variations (Andreev and Gramberg, 2002). The average Co concentrations of the stratigraphic sections of the Fe-Mn crusts from the Magellan seamounts range from 0.32% to 0.65% (Melnikov and Pletnev, 2013). Thus, it is essential to clarify the controls on the variations of Co concentration of Fe-Mn crusts to develop criteria for exploration and extraction.

Halbach et al. (1983) suggested that Co-flux is constant over one order of magnitude of Fe-Mn crust growth rates, and consequently concluded that extremely slow growth rates and high Mn concentrations result in high Co concentrations. Based on the growth rate and chemical compositions of Fe-Mn crusts from the mid-Pacific, Manheim (1986) proposed that Co fluxes were roughly constant regardless of the water depth, which indicates that slow growth rates will result in high Co concentration in Fe-Mn crusts. Ren et al.(2022, 2024) proposed that oxidizing deep-water, oligotrophic bottom currents, and low sedimentation rates are optimal for west Pacific Co-rich Fe-Mn nodule formations (similar to Fe-Mn crusts in chemistry and mineralogy) to enrich multiple elements from seawater, including Co. Hein et al. (2000) suggested that the dominant controls on the concentration of elements (including Co) in Fe-Mn crusts include the concentration of the elements in seawater, element-particle reactivity, element residence time in seawater, the absolute and relative amounts of Fe and Mn in Fe-Mn crusts, dilution from detrital and diagenetic minerals, the colloid surface charge and types of complexing agents, the value of x in MnO_{2-x}, dissolved O_2 and pH of seawater, specific surface area, and growth rate.

In this work, we analyze the potential controls for Co concentrations in Fe-Mn crusts from the Magellan seamounts, and propose an equation that unites all the factors.

2 Samples and methods

2.1 Sample description

Fe-Mn crusts from two sites are used here. Fe-Mn crust DY31-III-JL-Dive70C (hereafter Fe-Mn crust DY31) was collected by the Chinese submersible *Jiaolong* in 2013 on Caiwei seamount (Magellan seamounts) (155.5492° E, 15.9246° N) at a water depth of 2270 m. Fe-Mn crust MAD23 was collected by dredge on the *R. V. Dayang Yihao* in 2006 from Caiwei seamount (155.5284° E, 15.9124° N) at a water depth between 1904 m and 1885 m (Figure 1). Fe-Mn crust DY31 is about 6 cm thick, and the stratigraphic section can be divided into three distinct layers called II-1, II-2 and III (Figure 2). Layer II-1 is the lowermost layer, 1 cm thick, and shows a dendritic texture with dendrite orientation indicating that layer II-1 is an older crust that was turned over before layers II-2 and III were accreted on to it. The overlying layer II-2 is about 2 cm thick, black, and dense, with a dendritic texture composed of short dendrites oriented in the opposite direction to those in layer II-1. Layer III is about 3 cm thick, composed of long, black dendrites. The substrate rock was not recovered. Fe-Mn crust MAD23 is 6.6 cm thick, and the stratigraphic section is divided into three distinct layers from the bottom to the surface: I-1, II and III. Layer I-1 is 1.2 cm thick, dense, and black, with a laminated texture; layer II is 3.2 cm thick, dendritic, and varies from the compact to friable; layer III is 2.2 cm thick, black, and compact, with a dendritic texture (Figure 2).

2.2 Analytical methods for major elements, ^{230}Th isotope, and specific surface area of Fe-Mn crusts

In order to characterize the chemical composition, 20 samples were taken along the stratigraphic section of Fe-Mn crust DY31 (13 for layer III, 6 for layer II-2, and 1 for layer II-1); 21 samples were taken for Fe-Mn crust MAD23 (11 for layer III, 7 for layer II, and 3 for layer I-1) (Table 1). The outermost layers (youngest), 2.5 mm for Fe-Mn crust DY31 and 3.6 mm for Fe-Mn crust MAD23, are used in this study to investigate the controls on Co concentrations in Fe-Mn crusts. The samples were ground to a <74 μm powder in an agate mortar and pestle. The samples were then digested following the procedure described by Ren et al. (2010), and analyzed by Inductively Coupled Plasma Optical Emission Spectrometer (ICP-OES, Thermal iCAP6300 instrument) for Al_2O_3, CaO, TFe, K_2O, MgO, MnO_2, Na_2O, P_2O_5, TiO_2, Co, Cu, Ni, Ba, Sr, and Pb. Standards GSMC-1and GSMC-2 were analyzed together with Fe-Mn crust samples to monitor accuracy.

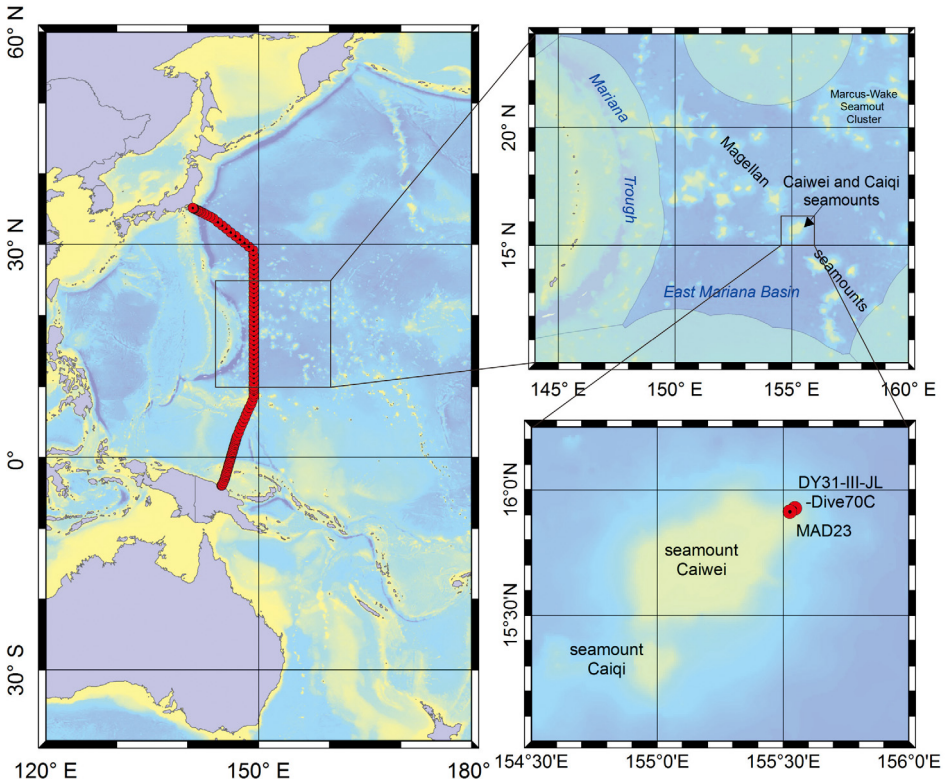

FIGURE 1
Left map, location of World Ocean Circulation Experiment (WOCE) P10 transect (red line); right top map, location of Caiwei seamount; and right bottom map, sampling sites of Fe-Mn crusts (red circles).

For determination of $^{230}Th_{ex}$ growth rates of the outermost layers of the Fe-Mn crusts, ten (DY31) and eight (MAD23) samples were scraped layer by layer with surgical blades from the outermost approximately 2 mm of crust (based on decay of ^{230}Th in Fe-Mn crusts and the detection limit). The sampling intervals d (mm) were calculated with the formula: $d(mm) = \frac{10 \times w(g)}{\rho(g/cm^3) \times A(cm^2)}$, where w is the weight of each sample; ρ is the density of Fe-Mn crusts (1.6 g/cm^3, Halbach et al., 1983), and A is the sampling area. The error of d is estimated to be ±20% (Ku et al., 1979). The samples were ground in an agate mortar and pestle and then dried at 110 ° C. Then the

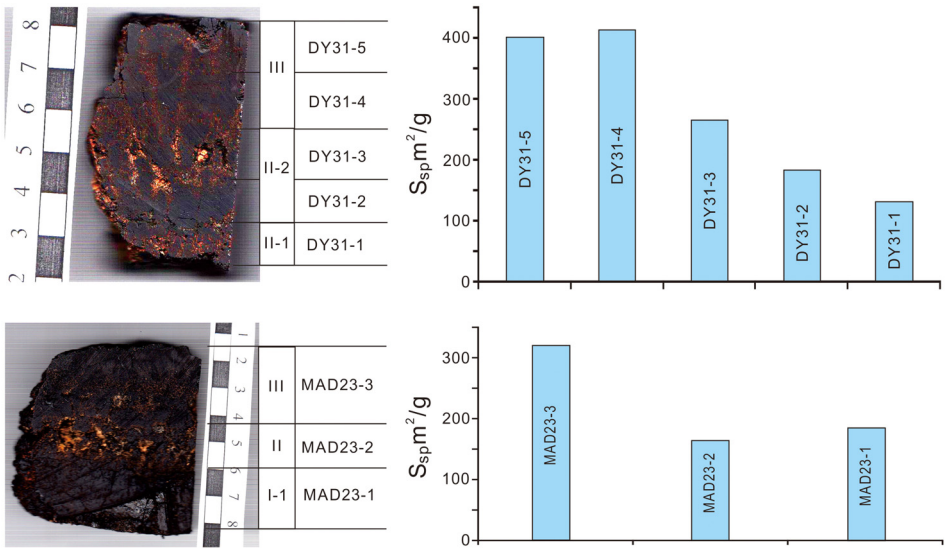

FIGURE 2
Variation of specific surface area in the stratigraphic sections of Fe-Mn crusts from Caiwei seamount; note the scale bars in cm divisions.

TABLE 1 Major element concentrations through stratigraphic sections of Fe-Mn crusts from Caiwei seamount of the Magellan seamounts.

Sample No.	Interval		Al_2O_3	CaO	TFe	K_2O	MgO	MnO_2	Na_2O	P_2O_5	TiO_2	Co	Cu	Ni	Ba	Sr	Pb
	mm		%														
DY31-III-JL-Dive70C: Layer III																	
Dive70C-(1)	0.0	2.5	2.4	2.9	15.9	0.77	1.95	34.5	2.23	0.84	2.2	0.67	0.24	0.49	0.20	0.14	0.17
Dive70C-(2)	2.5	4.7	1.5	3.4	17.5	0.56	1.68	32.2	2.13	0.86	1.6	0.68	0.06	0.33	0.13	0.14	0.16
Dive70C-(3)	4.7	7.1	1.5	3.0	17.8	0.56	1.69	31.5	2.16	0.81	1.6	0.63	0.07	0.33	0.14	0.15	0.16
Dive70C-(4)	7.1	9.1	1.5	2.9	17.5	0.55	1.63	32.0	2.15	0.79	1.6	0.62	0.08	0.34	0.14	0.14	0.15
Dive70C-(5)	9.1	11.6	1.4	2.8	17.2	0.55	1.61	32.9	2.17	0.80	1.6	0.64	0.09	0.36	0.14	0.14	0.15
Dive70C-(6)	11.6	14.1	1.5	3.0	16.7	0.59	1.69	32.9	2.17	0.76	1.8	0.61	0.11	0.37	0.14	0.15	0.15
Dive70C-(7)	14.1	15.6	1.5	3.0	16.3	0.57	1.64	33.2	2.15	0.76	1.8	0.59	0.13	0.39	0.15	0.14	0.15
Dive70C-(8)	15.6	18.2	1.7	3.0	17.8	0.62	1.75	36.3	2.38	0.85	2.1	0.62	0.16	0.44	0.16	0.15	0.16
Dive70C-(9)	18.2	20.8	1.6	2.9	15.7	0.59	1.63	31.8	2.00	0.71	1.9	0.47	0.14	0.37	0.15	0.14	0.18
Dive70C-(10)	20.8	22.5	1.8	3.0	17.0	0.63	1.67	32.2	2.12	0.73	2.0	0.45	0.16	0.37	0.16	0.15	0.14
Dive70C-(11)	22.5	25.1	2.1	2.9	18.7	0.63	1.64	30.3	2.10	0.78	2.0	0.43	0.16	0.33	0.17	0.15	0.15
Dive70C-(12)	25.1	27.2	2.3	2.8	18.6	0.64	1.61	29.6	2.08	0.77	1.8	0.44	0.17	0.32	0.17	0.14	0.14
Dive70C-(13)	27.2	30.8	2.4	2.9	17.3	0.71	1.76	31.0	2.12	0.73	1.9	0.52	0.18	0.36	0.17	0.14	0.13
DY31-III-JL-Dive70C: Layer II-2																	
Dive70C-(14)	30.8	33.8	2.7	3.0	15.0	0.83	1.98	34.0	2.15	0.70	2.1	0.64	0.22	0.47	0.17	0.14	0.11
DiIve70C-(15)	33.8	37.2	2.4	3.2	15.3	0.80	1.97	33.8	2.08	0.75	2.3	0.59	0.22	0.45	0.19	0.14	0.12
Dive70C-(16)	37.2	40.8	2.3	3.1	15.9	0.73	1.92	34.3	2.06	0.82	1.9	0.53	0.23	0.49	0.19	0.14	0.11
Dive70C-(17)	40.8	44.6	2.4	3.2	15.5	0.77	2.03	35.3	2.12	0.79	1.8	0.52	0.24	0.54	0.19	0.14	0.10
Dive70C-(18)	44.6	48.6	1.8	3.4	14.3	0.74	2.07	38.3	2.18	0.69	1.8	0.51	0.25	0.63	0.20	0.14	0.12
Dive70C-(19)	48.6	51.6	1.8	3.3	13.6	0.73	2.08	38.7	2.27	0.75	1.6	0.52	0.25	0.74	0.20	0.14	0.12
DY31-III-JL-Dive70C: Layer II-1																	
Dive70C-(20)	51.6	60.8	2.3	3.2	16.5	0.68	1.96	35.2	2.28	0.84	1.6	0.65	0.12	0.51	0.14	0.14	0.14
MAD23: Layer III																	
MAD23-(1)	0.0	3.6	5.5	3.5	18.8	0.63	1.92	29.7	2.62	1.03	1.4	0.53	0.04	0.32	0.12	0.14	0.15
MAD23-(2)	3.6	4.4	1.9	3.0	18.7	0.60	1.80	30.5	2.54	0.94	1.5	0.56	0.04	0.31	0.12	0.14	0.16
MAD23-(3)	4.4	5.2	1.8	2.9	18.7	0.61	1.78	30.4	2.46	0.95	1.5	0.59	0.05	0.31	0.12	0.14	0.16
MAD23-(4)	5.2	6.6	1.7	2.9	18.8	0.61	1.78	31.6	2.46	0.92	1.5	0.62	0.05	0.34	0.13	0.14	0.16
MAD23-(5)	6.6	9.0	1.6	3.0	17.9	0.62	1.83	32.3	2.47	0.83	1.6	0.68	0.06	0.38	0.14	0.15	0.15
MAD23-(6)	9.0	10.9	1.8	2.8	17.8	0.62	1.73	31.8	2.49	0.81	1.6	0.69	0.07	0.38	0.14	0.14	0.15
MAD23-(7)	10.9	13.5	2.0	2.8	17.2	0.64	1.70	31.7	2.54	0.79	1.6	0.71	0.07	0.39	0.14	0.13	0.15
MAD23-(8)	13.5	14.8	2.1	2.8	16.8	0.68	1.66	31.5	2.55	0.77	1.6	0.66	0.08	0.37	0.14	0.13	0.14
MAD23-(9)	14.8	17.6	1.9	3.0	16.9	0.68	1.74	32.3	2.49	0.76	1.8	0.63	0.09	0.37	0.14	0.14	0.14
MAD23-(10)	17.6	19.6	1.5	3.1	16.8	0.58	1.72	34.8	2.42	0.81	2.0	0.65	0.11	0.42	0.16	0.15	0.15
MAD23-(11)	19.6	22.6	1.3	3.2	16.8	0.58	1.77	36.1	2.42	0.77	2.1	0.62	0.13	0.44	0.17	0.16	0.16

(Continued)

10.3389/fmars.2024.1489943

TABLE 1 Continued

Sample No.	Interval		Al_2O_3	CaO	TFe	K_2O	MgO	MnO_2	Na_2O	P_2O_5	TiO_2	Co	Cu	Ni	Ba	Sr	Pb
	mm		%														
MAD23: Layer II																	
MAD23-(12)	22.6	23.0	1.6	3.1	17.5	0.63	1.82	33.8	2.36	0.77	2.1	0.56	0.14	0.42	0.18	0.15	0.16
MAD23-(13)	23.0	33.0	2.4	3.0	17.8	0.81	1.89	31.8	2.33	0.74	2.0	0.56	0.16	0.39	0.18	0.14	0.14
MAD23-(14)	33.0	39.0	2.5	3.2	16.6	0.85	2.01	34.1	2.27	0.84	2.3	0.61	0.18	0.44	0.21	0.14	0.12
MAD23-(15)	39.0	43.0	2.4	3.2	16.8	0.80	2.00	33.6	2.25	0.84	2.0	0.53	0.19	0.47	0.21	0.14	0.12
MAD23-(16)	43.0	45.5	1.6	3.4	15.6	0.68	1.98	37.9	2.36	0.76	2.0	0.56	0.21	0.57	0.21	0.15	0.13
MAD23-(17)	45.5	49.0	1.5	3.7	14.7	0.72	2.07	39.5	2.48	0.90	1.8	0.51	0.23	0.68	0.22	0.15	0.12
MAD23-(18)	49.0	53.8	1.9	4.2	15.9	0.71	1.92	36.5	2.44	1.41	1.6	0.37	0.20	0.55	0.23	0.15	0.14
MAD23: Layer I-1																	
MAD23-(19)	53.8	56.7	1.6	6.0	16.4	0.65	1.79	34.4	2.32	2.54	1.8	0.34	0.18	0.44	0.26	0.16	0.15
MAD23-(20)	56.7	59.4	1.3	10.3	13.8	0.60	1.70	33.7	2.27	5.19	1.8	0.39	0.18	0.46	0.26	0.17	0.14
MAD23-(21)	59.4	66.2	0.9	15.0	12.5	0.46	1.44	30.7	2.15	8.46	1.8	0.40	0.16	0.38	0.25	0.17	0.14

samples were digested following the procedure described by Hu et al. (2002). The digested samples were separated and purified using the procedure of Luo et al. (1986). U and Th isotopes were determined by alpha spectrometry (Octete ^{TM} PC).

To determine variations in specific surface area, eight samples were taken along the stratigraphic section of the Fe-Mn crusts in this study: five samples from Fe-Mn crust DY31 (two for layer III, two for layer II-2, and one for layer II-1) and three samples from layer III, II, and I-1 of Fe-Mn crust MAD23 (Figure 2). The samples were crashed to grains of about 1 mm in diameter, and then dried at 110 ° C. The specific surface areas were determined by N_2 adsorption using the BET method using a Belsorp-max instrument, in September 2014.

3 Results

3.1 Fe-Mn crusts cobalt and transition metals

The concentrations of Mn, Fe, Co, Ni, and Cu of Fe-Mn crusts DY31 and MAD23 show the same variations as those of other hydrogenetic Fe-Mn deposits (Table 1; Figure 3, right panel). The Co concentration of the outermost layer (2.5 mm) of DY31 is 0.67%, and MnO_2 concentration is 34.5%. The Co concentrations of layer III (0-30.8 mm) of this Fe-Mn crust range from 0.43% to 0.68% with a mean value of 0.57%. The Co concentrations of layer II-2 (30.8-51.6 mm) range from 0.51% to 0.64% with a mean value of 0.55%, and the Co concentration of layer II-1 (51.6-60.8 mm) is 0.65%. The Co concentration of the outermost layer (3.6 mm) of MAD23 is 0.53%, and MnO_2 concentration is 29.7%. The Co concentrations through the stratigraphic section of Fe-Mn crust MAD23 vary between 0.71% and 0.34%. The ranges of Co concentrations in MAD23 crust layer III (0-22.6 mm), II (22.6-53.8 mm), and I-1 (53.8-66.2 mm) are 0.53-0.71%, 0.37-0.61%, and 0.34-0.40% respectively. The average Co concentrations for crust MAD23 decreases from 0.63% in layer III, to 0.53% of layer II, to 0.38% of layer I-1 (Figure 3, left panel).

3.2 Growth rates of outermost layers of the Fe-Mn crusts

The $^{230}Th_{ex}$ and ratios of $^{230}Th_{ex}/^{232}Th$ of the Fe-Mn crusts show exponential decreases with depth (age) (Table 2). The growth rates (GR) were estimated by fitting the depth distributions of $^{230}Th_{ex}$ and $^{230}Th_{ex}/^{232}Th$ with the isotope decay equations $^{230}Th_{ex})_d = {}^{230}Th_{ex})_0 \cdot e - \frac{\lambda_{230}}{GR} d$ and $^{230}Th_{ex}/^{232}Th)_d = {}^{230}Th_{ex}/^{232}Th)_0 \cdot e - \frac{\lambda_{230}}{GR} d$, where d is sampling depth in the stratigraphic sections and λ_{230} is the decay constant of ^{230}Th (9.19×10^{-6} a^{-1}) (Figure 4).

The decay curve of $^{230}Th_{ex}$ of Fe-Mn crust DY31 shows a deflection at 0.74 mm (around 420 ka). The GR of this Fe-Mn crust derived from $^{230}Th_{ex}$ are 1.75 ± 0.13 mm/Myr between 0.00 mm and 0.74 mm, and 5.90 ± 0.83 mm/Myr between 0.74 mm and 1.99 mm in the stratigraphic section, whereas the GR of this Fe-Mn crust derived from $^{230}Th_{ex}/^{232}Th$ are slightly higher between 0 mm and 0.74 mm, 2.03 ± 0.17 mm/Myr, and the same within error between 0.74 mm and 1.99 mm, 5.22 ± 0.45 mm/Myr. In contrast, the growth rates of Fe-Mn crust MAD23 are constant between 0 mm to 1.9 mm, 2.82 ± 0.13 mm/Myr by $^{230}Th_{ex}$ and 2.77 ± 0.23 mm/Myr by $^{230}Th_{ex}/^{232}Th$.

3.3 Specific surface area of Fe-Mn crusts from Caiwei seamount

The specific surface area decreases with depth (age) through the stratigraphic sections of the two Fe-Mn crusts (Table 3; Figure 2).

10.3389/fmars.2024.1489943

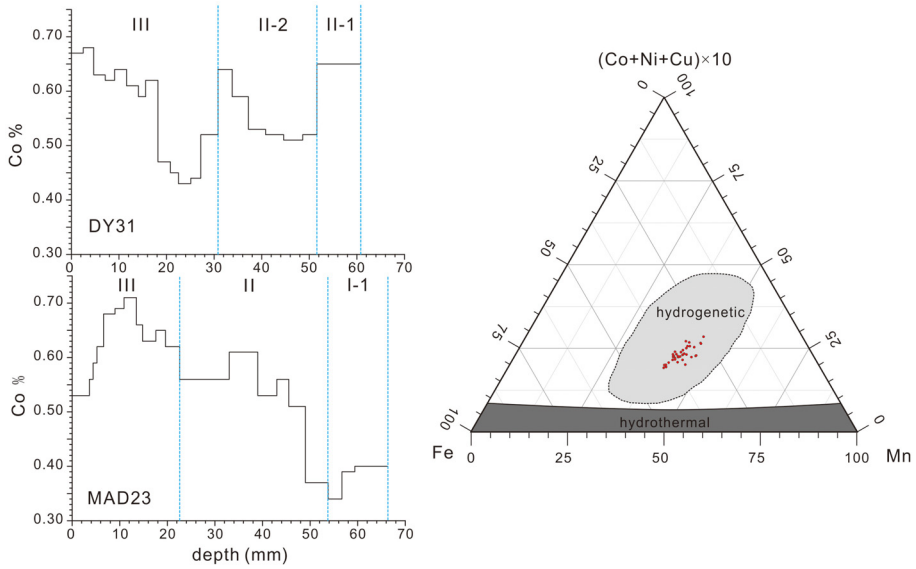

FIGURE 3
Left panel, Co concentrations of Fe-Mn crusts DY31 and MAD23 through the stratigraphic sections; right panel, ternary diagram of Mn, Fe, and (Cu +Co+Ni)×10 following Bonatti et al. (1972) for samples analyzed in this study.

TABLE 2 ^{238}U, ^{234}U, ^{230}Th, ^{232}Th, and $^{230}Th_{ex}$ specific activity, and the ratios $^{230}Th_{ex}/^{232}Th$ of Fe-Mn crusts from Caiwei seamount.

Sample No.	interval	Average depth	^{238}U	^{234}U	^{230}Th	^{232}Th	$^{230}Th_{ex}$	$^{230}Th_{ex}/^{232}Th$
	(mm)	(mm)	10^{-2} Bq/g					
DY31-III-JL-Dive70C								
Dive 70C-1	0-0.16	0.08	16.92 ± 1.48	18.55 ± 1.56	1207.20 ± 43.05	13.28 ± 0.87	1188.64 ± 43.08	89.50 ± 6.70
Dive 70C-2	0.16-0.34	0.25	15.71 ± 1.31	17.93 ± 1.42	468.43 ± 18.80	12.56 ± 0.89	450.50 ± 18.85	35.86 ± 2.96
Dive 70C-3	0.34-0.53	0.44	15.01 ± 1.10	15.74 ± 1.14	182.62 ± 7.80	9.77 ± 0.76	166.88 ± 7.89	17.08 ± 1.55
Dive 70C-4	0.53-0.74	0.63	14.54 ± 1.22	15.74 ± 1.29	105.83 ± 7.91	9.88 ± 1.21	90.09 ± 8.02	9.11 ± 1.38
Dive 70C-5	0.74-0.96	0.85	15.39 ± 1.24	15.79 ± 1.27	88.05 ± 6.79	11.04 ± 1.32	72.26 ± 6.91	6.54 ± 1.00
Dive 70C-6	0.96-1.15	1.05	15.82 ± 1.20	17.89 ± 1.31	95.63 ± 4.91	13.36 ± 1.01	77.74 ± 5.09	5.82 ± 0.58
Dive 70C-7	1.15-1.35	1.25	13.37 ± 1.25	16.67 ± 1.45	54.97 ± 3.20	12.66 ± 1.03	38.30 ± 3.52	3.02 ± 0.37
Dive 70C-8	1.35-1.56	1.45	17.56 ± 1.54	17.51 ± 1.54	39.77 ± 2.24	11.54 ± 0.89	22.26 ± 2.73	1.93 ± 0.28
Dive 70C-9	1.56-1.78	1.67	15.86 ± 1.30	14.01 ± 1.20	31.85 ± 1.95	13.25 ± 1.01	17.84 ± 2.29	1.35 ± 0.20
Dive 70C-10	1.78-1.99	1.89	13.26 ± 1.15	14.71 ± 1.22	28.83 ± 1.90	10.97 ± 0.93	14.12 ± 2.26	1.29 ± 0.23
MAD23								
MAD23-2-1	0-0.18	0.09	13.79 ± 0.99	21.85 ± 1.33	748.61 ± 21.60	10.21 ± 0.59	726.76 ± 21.65	71.21 ± 4.62
MAD23-2-2	0.18-0.42	0.3	16.58 ± 1.11	20.27 ± 1.27	376.73 ± 12.21	12.75 ± 0.73	356.47 ± 12.28	27.97 ± 1.87
MAD23-2-3	0.42-0.78	0.6	12.60 ± 0.97	17.22 ± 1.19	155.74 ± 5.06	9.98 ± 0.52	138.52 ± 5.20	13.88 ± 0.90
MAD23-2-4	0.78-1.04	0.91	13.13 ± 0.79	16.80 ± 0.92	55.34 ± 2.03	10.32 ± 0.57	38.53 ± 2.24	3.73 ± 0.30
MAD23-2-5	1.04-1.29	1.16	12.03 ± 0.69	12.21 ± 0.70	47.46 ± 2.48	10.90 ± 0.72	35.25 ± 2.57	3.23 ± 0.32
MAD23-2-6	1.29-1.56	1.42	12.19 ± 0.79	14.08 ± 0.88	25.07 ± 1.34	9.39 ± 0.61	11.00 ± 1.66	1.17 ± 0.19
MAD23-2-7	1.56-1.71	1.64	18.17 ± 1.35	18.90 ± 1.39	–	–	–	–
MAD23-2-8	1.71-1.90	1.81	15.04 ± 1.01	16.60 ± 1.08	–	–	–	–

"-" means below detection limit.

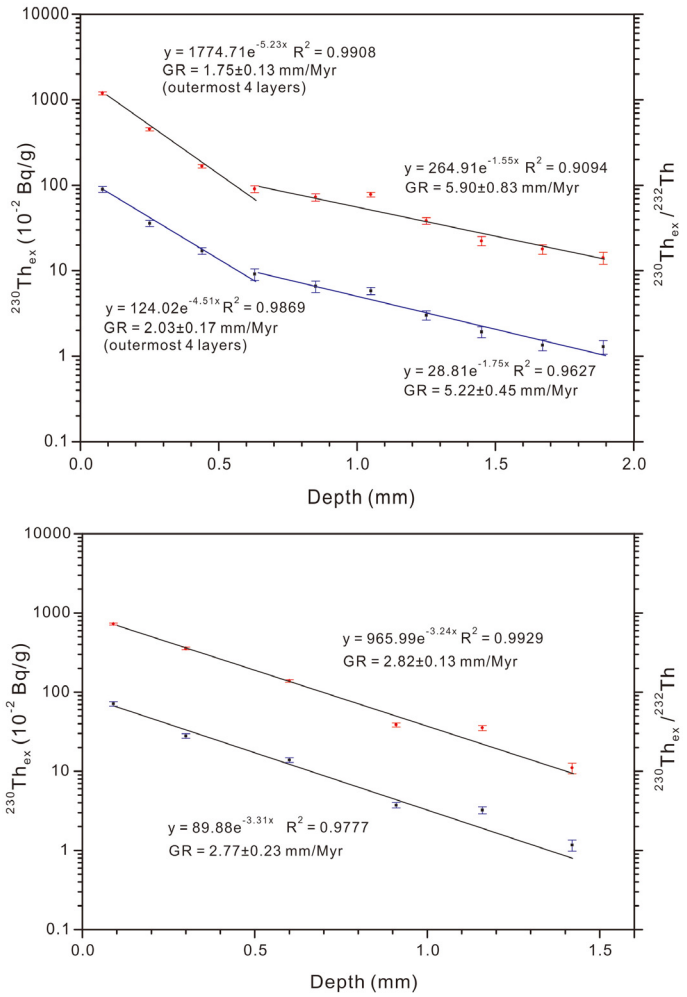

FIGURE 4
Fe-Mn crusts DY31 (top panel) and MAD23 (bottom panel) from Caiwei seamount, decay profiles of $^{230}Th_{ex}$ activities (upper curves, red dots in each panel) and $^{230}Th_{ex}/^{232}Th$ activities (lower curve, blue dots in each panel), error bars are shown for each datum.

The specific surface areas of DY31 decrease from 401 m^2/g and 414 m^2/g in the upper and lower parts of layer III respectively, to 266 m^2/g and 185 m^2/g in the upper and lower parts of layer II-2, to 132 m^2/g in layer II-1 (Figure 2, top panel). The specific surface areas of MAD23 decrease from 321 m^2/g in layer III, to 165 m^2/g in layer II, and about the same in layer I-1, 185 m^2/g (Figure 2, bottom panel). Fe-Mn crust DY31 was kept moist after recovery from Caiwei seamount, and determined one year after recovery, while Fe-Mn crust MAD23 was stored dry and analyzed 8 years after recovery. The Fe-Mn crust analyzed soon after collection has higher specific surface areas relative to those analyzed later.

4 Discussion

4.1 Theoretical model for the controls of cobalt in Fe-Mn crusts

Almost all of the Co in seawater from the western North Pacific is dissolved rather than particulate (Nakatsuka et al., 2009). The two main species of dissolved Co in seawater are Co^{2+} (65%) and $CoCl^+$ (14%) (Byrne, 2002). Those Co ions are transported with bottom currents and diffuse onto the surface of Fe-Mn crusts, where Co^{2+} ions are adsorbed by δ-MnO_2 (98-99%; Koschinsky and Hein, 2003) and oxidized to Co^{3+}, initially proposed by Murray and Dillard (1979). In this Co enrichment process, diffusion is the critical step because of the low diffusion flux relative to its oxidation rate by δ-MnO_2. Halbach et al. (1983) estimated that the fluxes of Co into Fe-Mn crusts from the Line Islands are 2.4-4.0 μg cm^{-2} kyr^{-1}; in their calculation, the high specific surface area of Fe-Mn crusts (average 300 m^2/g; Hein et al., 2000) was not incorporated, which can decrease the Co flux. Kanungo et al. (2004) carried out adsorption experiments of Co on hydrous manganese dioxide from complex electrolyte solutions resembling seawater in major ion concentrations, and the results show that δ-MnO_2 adsorbed 2.4 mmole/g Co in 72 hours at pH 7.25 and temperature of 300 K. The specific surface areas of δ-MnO_2 used in that study range from 2.64 m^2/g to 94.22 m^2/g (Parida et al., 1981). Consequently, we calculated the maximum adsorption flux of Co on the surface of δ-MnO_2 to be about 1.62×10^6 μg cm^{-2} kyr^{-1}, which is much higher

TABLE 3 Specific surface area of stratigraphic sections of Fe-Mn crusts from Caiwei seamount.

Aliquot No.	Stratigraphic layer	Sampling interval	Specific surface area	Total volume
		mm	m^2/g	cm^3/g
DY31-III-JL-Dive70C (155.5492°E, 15.9246°N; water depth 2270 m; sampling date: September 4, 2013)				
DY31-III-JL-DIve70C-5	III	1.2	401.08	0.1966
DY31-III-JL-DIve70C-4	III	1.3	414.94	0.2041
DY31-III-JL-DIve70C-3	II-2	1.2	266.26	0.1415
DY31-III-JL-DIve70C-2	II-2	1.3	184.75	0.0917
DY31-III-JL-DIve70C-1	II-1	0.6	131.81	0.0710
MAD23 (155.5294°E, 15.9102°N; water depth 1895 m;, sampling date: June 6, 2006)				
MAD23-3	III	3.0	321.15	0.1579
MAD23-2	II	1.3	165.15	0.0816
MAD23-1	I-1	2.7	185.49	0.0915

than the Co fluxes on Fe-Mn crusts in the natural seawater system. This difference in Co flux may result mainly from the different Co concentrations in the laboratory solution and in seawater. Nevertheless, the adsorption experiment shows the great potential of Fe-Mn crusts to adsorb Co. Therefore, based on flux data and adsorption capacity, it is reasonable to conclude that the diffusion of Co in seawater is the critical step in the Co enrichment process from seawater to Fe-Mn crusts.

Assuming that all the Co ions that diffused to the surface of the Fe-Mn crusts were adsorbed and eventually captured through surface oxidation by the Fe-Mn crusts, the concentrations of Co in the Fe-Mn crusts (C_{cr}, assuming that the concentration of δ-MnO_2 in Fe-Mn crusts is equal to the percentage of MnO_2; Co concentration in Fe-Mn crusts normalized to MnO_2 = 100% to eliminate dilution mainly from detrital minerals and FeOOH) can be given by

$$C_{cr} = J \cdot S_{sp} \cdot \int_0^t dt \quad (1)$$

Where J = diffusion flux of Co, S_{sp} = specific surface area of the Fe-Mn crusts, and $\int_0^t dt$ = duration for the growth of one molecular layer.

When J is the function of time t, Equation 1 should be rewritten as

$$C_{cr} = \int_0^t J \cdot S_{sp} dt \quad (2)$$

For a semi-infinite medium with constant surface concentration, the concentration can be derived from Albarede (1995) as

$$C = (C_0 - C_{int})erf\frac{x}{2\sqrt{Dt}} + C_{int} \quad (3)$$

Where C = concentration in a semi-infinite medium, $C_{int} = C$ at $x = 0$, $C_0 = C$ at $x = \infty$, D = diffusivity. Based on Equation 3, the response time and gradient of concentration C to the surface concentration C_{int} can be estimated for Co diffusion in deep-sea water in a diffusion layer of 5 mm as shown in Figure 5, where C_{int} = 34.1 pM, $C_0 = 0$, $D = 3.626\times10^{-6}$ cm^2/s for this research (shown in section 4.2.2 and 4.2.3). Figure 5 shows that the gradient of the concentration of Co in the diffusion layer is nearly constant when time t = 1000 s, which indicates that the response time of Co concentration in the diffusion layer is rather short. In this case with a constant gradient of concentration Co, the diffusion can be described by Fick's First Law. Since deep seawater is a dissipative system, it is reasonable to assume that the Co concentration in ambient seawater of seamounts vary slowly relative to the short response time of the diffusion layer. Hence, we can use Fick's First Law to describe Co diffusion near the ferromanganese crusts on seamounts concisely.

Based on Fick's First Law, the diffusion flux of Co (J) from seawater to the Fe-Mn crusts can be given by

$$J = -D_{sw} \cdot \frac{dC_{sw}}{dx} \quad (4)$$

Where D_{sw} = diffusivity of Co ion in seawater, C_{sw} = Co ion concentration in seawater at time t, $\frac{dC_{sw}}{dx}$= diffusion gradient of Co ions. D_{sw} can be estimated by $D_{sw} = (m_0 + m_1T)\times10^{-6}$ cm^2/s, where m_0 = 3.31, m_1 = 0.158, and T is temperature in Celsius (Boudreau, 1997). Assuming that the Co concentration in seawater near the interface of seawater and Fe-Mn crusts is 0 and the diffusion distance of Co ions near the interface is δ, then the $\frac{dC_{sw}}{dx} = -\frac{C_{sw}}{\delta}$.

The duration for the growth of one molecular layer of Fe-Mn crust t can be given by

$$t = \frac{z}{GR} \quad (5)$$

Where z = the thickness of one molecular layer of Fe-Mn crust (4.7Å, Manheim, 1986), GR = growth rate.

When the Equations 2, 4, and 5 are combined, the concentration of Co in Fe-Mn crusts (C_{cr}) can be given by

$$C_{cr} = \int_0^{\frac{z}{GR}} D_{sw} \cdot \frac{C_{sw}}{\delta} \cdot S_{sp} \cdot dt \quad (6)$$

Where C_{sw} is not constant in the duration for the growth of one molecular layer and varies with time t.

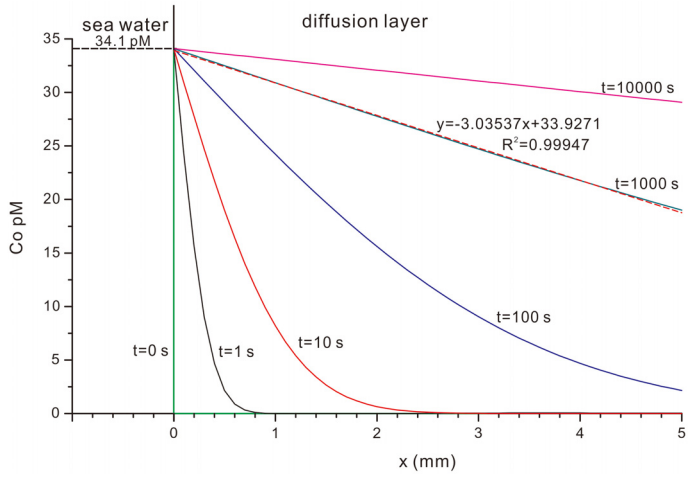

FIGURE 5
Response time and gradient of Co concentrations in the diffusion layer to the surface concentration.

When C_{sw} is constant in the duration for the growth of one molecular layer, Equation 4 can be rewritten as

$$C_{cr} = D_{sw} \cdot \frac{C_{sw}}{\delta} \cdot S_{sp} \cdot \frac{z}{GR} \quad (7)$$

When C_{sw} is not constant in the duration for the growth of one molecular layer, Equation 4 can be rewritten as

$$\overline{C_{cr}} = D_{sw} \cdot \frac{\overline{C_{sw}}}{\delta} \cdot S_{sp} \cdot \frac{z}{GR} \quad (8)$$

Where $\overline{C_{sw}}$ is the averaged C_{sw} weighted by time t, and $\overline{C_{cr}}$ is the averaged Co concentration derived from $\overline{C_{sw}}$.

Equations 5, 6 indicate that the controls on the Co concentrations in Fe-Mn crusts include diffusivity of Co ions in seawater (D_{sw}), temperature which controls the D_{sw}, Co ion concentration in seawater (C_{sw} or $\overline{C_{sw}}$), the diffusion distance of Co ions near the interface of seawater and Fe-Mn crusts (δ), growth rate (GR), and specific surface area of Fe-Mn crusts (S_{sp}).

4.2 Estimation of parameters

In Equations 7, 8, the diffusion distance of Co ions near the interface of seawater and Fe-Mn crusts (δ) cannot be measured directly. Therefore, we calculated δ for the Fe-Mn crusts from Caiwei seamount based on Co concentrations, growth rates, and specific surface area of the outermost layer of the Fe-Mn crusts, diffusivity of Co^{2+}, and Co concentration in the seawater.

4.2.1 Major elements

The sequential leaching experiments (Koschinsky and Halbach, 1995; Koschinsky and Hein, 2003) and X-ray absorption near-edge structure data (Takahashi et al., 2007) show that the Co in Fe-Mn crusts resides in vernadite (δ-MnO_2). Consequently, the other minerals in Fe-Mn crusts, such as aluminosilicates, phosphates, and FeOOH dilute the Co concentration of Fe-Mn crusts. In order to eliminate the dilution parameter, we normalized the Co concentration to 100%MnO_2. The normalized Co concentrations of the outermost layers of DY31 (2.5 mm) and MAD23 (3.6 mm) are 2.14% and 1.79% respectively.

4.2.2 Diffusivity of Co ions in seawater (D_{sw})

The modern seawater temperature is 2°C at 2000 m water depth around Caiwei seamount (Figure 6). The diffusivity of Co ions in seawater is estimated to be 3.626×10^{-6} cm^2/s by $D_{sw} = (m_0 + m_1T)\times10^{-6}$ cm^2/s, where m_0 = 3.31, m_1 = 0.158, and T is in Celsius (Boudreau, 1997).

4.2.3 Specific surface area

In Equations 7, 8, the specific surface area of δ-MnO_2 should be used to calculate δ. However, the specific surface area of δ-MnO_2 is difficult to determine separately from FeOOH, which is epitaxially intergrown. The vernadite (δ-MnO_2) in Fe-Mn crusts from the western Pacific are sheets as thin as 1 nm determined by Aberration-corrected FEG-STEM, and ferrihydrite (FeOOH) is typically 10 nm or less in diameter (Hochella, 2008), both of which coexist at a less than 1 micron scale as shown by EPMA with a spot diameter of 1 μm, which can detect the X-ray signals from Mn and Fe simultaneously (e.g. Ren et al., 2011).

The specific surface areas (S_{sp}) in this study were determined for Fe-Mn crusts, which predominantly reflect δ-MnO_2 and FeOOH. The specific surface areas of surface samples (≤ 1 mm sampling depth) and volume samples (≤ 5-6 mm sampling depth) of Fe-Mn crusts from Karin Ridge of the Mid-Pacific Mountains vary from 250 m^2/g to 381 m^2/g, and decreased up to 20% and 40% during the first four weeks and the eight weeks respectively after collection (Hein et al., 1994). The specific surface area along the section of a Fe-Mn crust from Marshall Islands range from 373 m^2/g to 530 m^2/g for the younger generation, and from 84 m^2/g to 178 m^2/g for the older generation (Xue, 2007). The specific surface areas for Fe-Mn crusts DY31 and MAD23 in this study show the same variations as those obtained by Hein et al. (1994) and Xue (2007). The specific surface

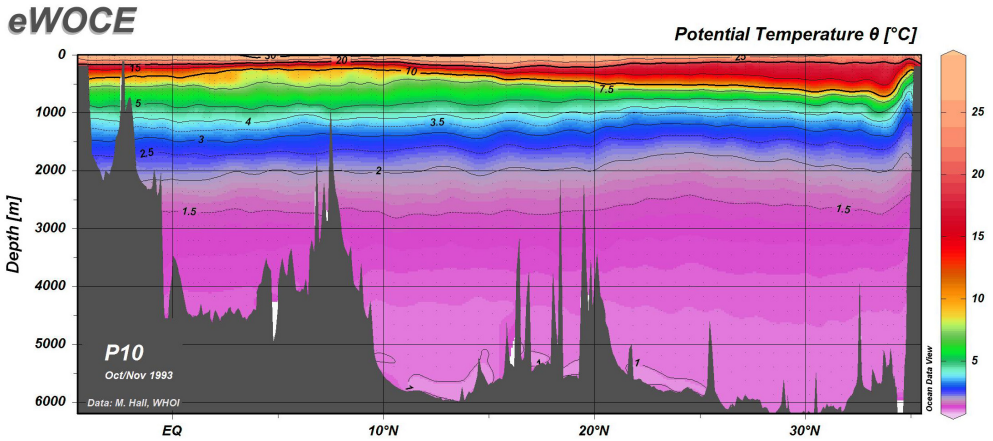

FIGURE 6
Profile of seawater temperature, west Pacific (location is shown in left map of Figure 1; modified with permission after http://www.ewoce.org/gallery/P10_TPOT.gif, Schlitzer, Reiner, Electronic Atlas of WOCE Hydrographic and Tracer Data Now Available, Eos Trans. AGU, 81(5), 45, 2000).

areas of the younger generations are greater than those of the older generation; the specific surface areas of MAD23 8-years after collection are lower than those measured 1 year after collection (Figure 7). The variation of specific surface areas reflects differences in stratigraphy and preservation. From these data, we infer that only the well-preserved outermost layers of Fe-Mn crusts can be used to obtain specific surface areas that may closely reflect those existing under *in situ* conditions. Specific surface area shows a nearly perfect positive correlation (r = 0.997) with pore volume, with an intercept close to zero (Figure 7), which indicates that the same characteristic or process may control both, such as particle size. These considerations indicate that it is most appropriate to use the S_{sp} of the outermost layer of crust DY31 to estimate the δ in Equations 7, 8.

4.2.4 Growth rate by $^{230}Th_{ex}$

The plots of $^{230}Th_{ex}$ and $^{230}Th_{ex}/^{232}Th$ versus depth show constant exponential decay curves for Fe-Mn crusts DY31 (0-0.74 mm) and MAD23 (0-1.99 mm), indicating that the growth rates were constant during the growth of these outermost layers for each crust. Therefore, we assume that the growth rates for modern Fe-Mn crusts are the same as those that define the growth rates of the outermost layers approximately 0.74 mm and 2 mm for DY31 and MAD23 respectively. Here we use 1.75 mm/Myr ($^{230}Th_{ex}$) and 2.03 mm/Myr ($^{230}Th_{ex}/^{232}Th$) for Fe-Mn crust DY31, and 2.82 mm/Myr ($^{230}Th_{ex}$) and 2.77 mm/Myr ($^{230}Th_{ex}/^{232}Th$) for Fe-Mn crust MAD23 to estimate δ in Equations 7, 8.

4.2.5 Estimation of diffusion gradients of Co ions ($\overline{C_{sw}}/\delta$)

Using the above parameters, the diffusion gradients of Co ions ($\overline{C_{sw}}/\delta$) can be estimated (Table 4). Based on the parameters for Fe-Mn crust DY31, the diffusion gradient of Co ions ranges from 295 pM/mm to 342 pM/mm. The gradient calculated for Fe-Mn crust MAD23 is greater than for DY31, ranging from 487 pM/mm to 496

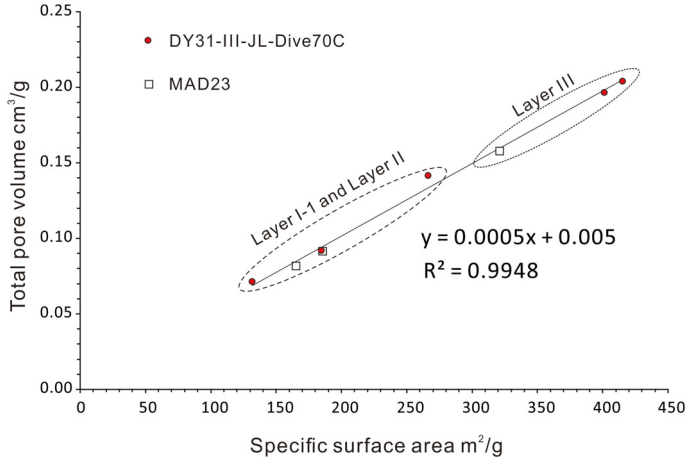

FIGURE 7
Regression of specific surface area versus total pore volume.

TABLE 4 Parameters used for calculation of diffusion gradients of Co ions $(\overline{C_{sw}}/\delta)$.

		DY31	MAD23	
Water depth	m	2270	1895	sampling water depth of Fe-Mn crusts
Thickness	mm	2.5	3.6	thickness of outermost layers in this study
MnO_2	%	35.48	29.69	MnO_2 concentration of Fe-Mn crust
Co	%	0.76	0.53	Co concentration of Fe-Mn crust
$\overline{C_{cr}}$	%	2.14	1.79	Co concentration, normalized to MnO_2 = 100%
S_{sp}	m^2/g	401.08	321.15	layer III
GR_1	mm/Myr	1.75	2.82	growth rate of outermost layer, determined by $^{230}Th_{ex}$
GR_2	mm/Myr	2.03	2.77	growth rate of outermost layer, $^{230}Th_{ex}/^{232}Th$
z	Å	4.7	4.7	thickness of one molecular layer
D_{sw}	10^{-6} cm^2/s	3.626	3.626	diffusivity of Co ions in seawater
$\overline{C_{sw}}/\delta$	pM/mm	295	496	using GR_1
	pM/mm	342	487	using GR_2

pM/mm. Given the bottom currents and mixing generated by the impact of water masses on seamounts (e.g., Lueck and Mudge, 1997), and the Co ion concentrations of seawater below 2000 m in the Pacific ranging from approximately 30 pM to 40 pM, the diffusion gradients of Co ions obtained in this study are reasonable.

4.3 Controls on the decreased Co concentrations with water depth

The Co concentrations of Fe-Mn crusts decrease with water depth. For example, the Co concentrations of Fe-Mn crusts from Line Islands decrease by 69% with increasing water depth, from 2.0% at 1120 m to 0.62% at 3280 m (Halbach et al., 1983). Data from Cronan (1977) also show that Co concentrations of Fe-Mn crusts decrease by more than 50% from 1000 m to 3000 m. The average Co concentrations of Fe-Mn crusts from the global ocean (Andreev and Gramberg, 2002) decrease from around 0.75% at 1000 m to 0.25% at 4000 m, a 66% decrease.

According to Equation 8, the Co concentration in Fe-Mn crusts can be given by

$$\mathrm{Co}(\%) = \mathrm{MnO_2}(\%) \cdot \mathrm{D_{sw}} \cdot \frac{\mathrm{C_{sw}}}{\delta} \cdot \frac{\mathrm{z}}{\mathrm{GR}} \cdot \mathrm{S_{sp}} \quad (9)$$

The statistical data show that no significant correlation exists between water depth and growth rates of surface samples of Fe-Mn crusts (Hein et al., 2000). The specific surface areas of Fe-Mn crusts from Karin Ridge of the central Pacific do not show a significant correlation with water depth (Hein et al., 1994). Furthermore, z and δ are constant in Equation 9. So in this study we only consider the D_{sw}, C_{sw} and MnO_2 concentration (dilution effects).

The seawater Co concentrations (C_{sw}) decrease from around 38 pM at 2000 m to around 32 pM at 4000 m, a decrease of 16% (Biller and Bruland, 2012); the Co diffusivity (D_{sw}) decreases from 3.626×10^{-6} cm^2/s (2000 m and 2°C) to 3.468×10^{-6} cm^2/s (around 4500 m and 1°C), a decrease of 4.4%. So, integration of the decreases of D_{sw} and C_{sw} can decrease Co concentration of Fe-Mn crusts by 20% of the original value from shallow water to deep water, which is not enough to account for the measured deceases of Co concentrations of Fe-Mn crusts with increasing water depth. Therefore, we infer that the decrease of MnO_2 concentration through dilution from aluminosilicates and FeOOH should be the major control, which is consistent with the conclusions of other studies. Halbach and Puteanus (1984) attributed the high Co concentration in the Fe-Mn crusts from shallow water (1500-1000 m) to the lower carbonate dissolution rates and correspondingly lower Fe supply to the crusts.

Equation 9 defines the controls on Co concentrations in the layers of Fe-Mn crusts as they were accreted. However, in most cases, only bulk Co concentrations in Fe-Mn crusts are available to quantify resources. The bulk Co concentrations are mathematically equal to the weighted average of those in various layers of Fe-Mn crusts, which can be affected by absence of some layers that were eroded as noted before by Hein et al. (2000). Bulk concentrations may also be influenced by the subsidence and migration of seamounts, which can change the ambient seawater chemical conditions around seamounts, even if the seawater chemistry was constant (as in the present oceans) during the growth of Fe-Mn crusts through the Cenozoic. Nevertheless, based on Equation 9, it is possible to ascertain the sensitivity of Co concentration to those potential influences for each stratigraphic interval. The controls including dilution effect from incorporation of detrital minerals (Kim et al., 2006) or dissolution of carbonate (Halbach and Puteanus, 1984), seawater Co concentrations (C_{sw}), and diffusivity (D_{sw}) vary continuously in the region of a seamount. When the Co concentrations in Fe-Mn crusts from a seamount are sensitive to those controls, Equation 9 can constitute the theoretical foundation for the application of Kriging to interpolate Co grade values and estimate the resources for each stratigraphic generation.

5 Summary and conclusions

Eight controls on Co concentrations in nonphosphatized Fe-Mn crusts are evaluated, including dilution effects, diffusivity of Co ions in seawater (D_{sw}), temperature which controls the D_{sw}, Co ion concentration in seawater (C_{sw}), the diffusion distance of Co ions near the interface of seawater and Fe-Mn crusts (δ), the thickness of one molecular layer of Fe-Mn crusts (z), growth rate (GR), and specific surface area of Fe-Mn crusts (S_{sp}). Those controls are integrated in the equation: $C_{cr} = D_{sw} \cdot \frac{C_{sw}}{\delta} \cdot \frac{z}{GR} \cdot S_{sp}$. Based on Co concentrations, growth rates, and specific surface area of the outermost layer of the Fe-Mn crusts, and diffusivity of Co^{2+}, the Co diffusion gradients ($\overline{C_{sw}}/\delta$) for the Fe-Mn crusts from Caiwei seamount is estimated to be 295-496 pM/mm. According to the model developed here, the decrease of Co concentration in Fe-Mn crusts with increasing water depth is controlled mainly by dilution of MnO_2, the main Co host-, and to a lesser extent seawater Co ion concentration, temperature, and consequently the diffusivity of Co ions in seawater.

Data availability statement

The raw data supporting the conclusions of this article will be made available by the authors, without undue reservation.

Author contributions

XR: Conceptualization, Funding acquisition, Investigation, Project administration, Visualization, Writing – original draft, Writing – review & editing. JH: Writing – review & editing. ZY: Methodology, Writing – review & editing. NX: Methodology, Writing – review & editing. AZ: Methodology, Writing – review & editing.

Funding

The author(s) declare financial support was received for the research, authorship, and/or publication of this article. This work was supported by the Marine S&T Fund of Shandong Province for Laoshan Laboratory (grant number: LSKJ202203600-2), by the China Ocean Mineral Resources R&D Association (COMRA) project (grant number: DY135-N2-1-04), and by the National Natural Science Foundation of China (grant number: 40806027).

Conflict of interest

The authors declare that the research was conducted in the absence of any commercial or financial relationships that could be construed as a potential conflict of interest.

Publisher's note

References

Albarede, F. (1995). *Introduction to geochemical modeling* (Cambridge: Cambridge University Press). doi: 10.1017/CBO9780511622960.010

Andreev, S. I., and Gramberg, I. S. (2002). *Cobalt-rich ores of the world ocean* (St. Petersburg: VNIIOkeageologia).

Benites, M., González, F. J., Hein, J., Marino, E., Reyes, J., Millo, C., et al. (2023). Controls on the chemical composition of ferromanganese crusts from deep-water to the summit of the Rio Grande Rise, South Atlantic Ocean. *Mar. Geol.* 462, 107094. doi: 10.1016/j.margeo.2023.107094

Biller, D. V., and Bruland, K. W. (2012). Analysis of Mn, Fe, Co, Ni, Cu, Zn, Cd, and Pb in seawater using the Nobias-chelate PA1 resin and magnetic sector inductively couples plasma mass spectrometry (ICP-MS). *Mar. Chem.* 130-131, 12–20. doi: 10.1016/j.marchem.2011.12.001

Bonatti, E., Kraemer, T., and Rydell, H. S. (1972). "Classification and genesis of submarine iron-manganese deposits," in *Ferromanganese Deposits on the Ocean Floor*. Ed. D. R. Horn (Washington, D. C.: Columbia University), 149–166.

Boudreau, B. P. (1997). *Diagenetic models and their implementation* (Berlin: Springer). doi: 10.1007/978-3-642-60421-8

Byrne, R. H. (2002). Inorganic speciation of dissolved elements in seawater: the influence of pH on concentration ratios. *Geochem. Trans.* 3, 11–16. doi: 10.1186/1467-4866-3-11

Cronan, D. S. (1977). "Deep-sea nodules: Distribution and geochemistry," in *Marine Manganese Deposits*. Ed. G. P. Glasby (Elsevier, Amsterdam), 11–44. doi: 10.1016/s0422-9894(08)71016-x

Halbach, P., and Puteanus, D. (1984). The influence of the carbonate dissolution rate on the growth and composition of Co-rich ferromanganese crusts from Central Pacific seamount areas. *Earth Planet. Sci. Lett.* 68, 73–87. doi: 10.1016/0012-821x(84)90141-9

Halbach, P., Segl, M., Puteanus, D., and Mangini, A. (1983). Co-flux and growth rates in ferromanganese deposits from central Pacific seamount areas. *Nature* 304, 716–719. doi: 10.1038/304716a0

Hein, J. R., Bychkov, A. S., and Gibbs, A. E. (1994). *Data and results from R.V. Aleksandr Vinogradov cruises 91-AV-19/1, North Pacific hydrochemistry transect; 91-av-19/2, North Equatorial Pacific Karin Ridge Fe-Mn crust studies; and 91-AV-19/4, Northwest Pacific and Bering sea sediment geochemistry and paleoceanographic studiest*. U.S. Geological Survey Open File Report Washington D.C.: Department of the Interior, 94–230. doi: 10.3133/ofr94230

Hein, J. R., and Koschinsky, A. (2014). "Deep-ocean ferromanganese crusts and nodules," in *Treatise on geochemistry, second edition, V. 13, Chapter 11*. Eds. H. D. Holland and K. K. Turekian (Oxford: Elsevier Ltd.), 273–291. doi: 10.1016/b978-0-08-095975-7.01111-6

Hein, J. R., Koschinsky, A., Bau, M., Manheim, F. T., Kang, J.-K., and Roberts, L. (2000). "Cobalt-rich ferromanganese crusts in the pacific," in *Handbook of Marine Mineral Deposits*. Ed. D. S. Cronan (CRC Press, Boca Raton, Florida), 239–279. doi: 10.1201/9780203752760-9

Hein, J. R., Mizell, K., Koschinsky, A., and Conrad, T. A. (2013). Deep-ocean mineral deposits as a source of critical metals for high- and green-technology applications: Comparison with land-based resources. *Ore. Geol. Rev.* 51, 1–14. doi: 10.1016/j.oregeorev.2012.12.001

Hochella, M. F. J. (2008). Nanogeoscience: From origins to cutting-edge application. *Elements* 4, 373–379. doi: 10.2113/gselements.4.6.373

Hu, G. L., Cai, Y. H., Yang, C. Y., Zhuang, Z. X., Wang, X. R., and Huang, Y. P. (2002). Determination of 27 elements in two polymetallic nodule reference samples from the Pacific Ocean by ICP-MS. *Acta Oceanol. Sin.* 24, 47–52. doi: 10.1007/s11670-002-0022-7

IEA (2021). *The Role of Critical Minerals in Clean Energy Transitions* (Paris: IEA). Available at: https://www.iea.org/reports/the-role-of-critical-minerals-in-clean-energy-transitions (Accessed November 13, 2023).

Kanungo, S. B., Tripathy, S. S., and Rajeev, (2004). Adsorption of Co, Ni, Cu, and Zn on hydrous manganese dioxide from complex electrolyte solutions resembling sea water in major ion content. *J. Colloid. Interface Sci.* 269, 1–10. doi: 10.1016/s0021-9797(03)00464-8

Kim, J., Hyeong, K., Jung, H., Moon, J., and Kim, K. (2006). Southward shift of the Intertropical Convergence Zone in the western Pacific during the late Tertiary: Evidence from ferromanganese crusts on seamounts west of the Marshall Islands. *Paleoceanography* 21, PA4218. doi: 10.1029/2006pa001291

Koschinsky, A., and Halbach, P. (1995). Sequential leaching of marine ferromanganese precipitates: Genetic implications. *Geochim. Cosmochim. Acta* 59, 5113–5132. doi: 10.1016/0016-7037(95)00358-4

Koschinsky, A., and Hein, J. R. (2003). Uptake of elements from seawater by ferromanganese crusts: solid-phase associations and seawater speciation. *Mar. Geol.* 198, 331–351. doi: 10.1016/S0025-3227(03)00122-1

Ku, T. L., Omura, A., and Chen, P. S. (1979). "Be^{10} and U-series isotopes in Mn nodules from the central North Pacific," in *Marine Geology and Oceanography of the Pacific Manganese Nodule Province*. Eds. J. L. Bishop and Z. Piper (Plenum, New York), 791–814. doi: 10.1007/978-1-4684-3518-4_26

Lueck, R. G., and Mudge, T. D. (1997). Topographically induced mixing around a shallow seamount. *Science* 276, 831–833. doi: 10.1126/science.276.5320.1831

Luo, S. D., Shi, W. Y., Chen, Z., and Huang, Y. P. (1986). Study on a new method for Separation and determination of U and Th in deep sea manganese nodules. *Acta Oceanol. Sin.* 8 (3), 324–330. Available at: http://www.hyxbocean.cn//cn/article/pdf/preview/19860309.pdf (Accessed August 2, 2024).

Manheim, F. T. (1986). Marine cobalt resources. *Science* 232, 600–608. doi: 10.1126/science.232.4750.600

Melnikov, M. E., and Pletnev, S. P. (2013). Age and formation conditions of the Co-rich manganese crust on guyots of the Magellan seamounts. *Lithol. Miner. Resour.* 48, 3–16. doi: 10.1134/s0024490212050057

Milesi, J.-P., Toteu, S. F., Deschamps, Y., Feybesse, J. L., Catherine, L., Cocherie, A., et al. (2006). An overview of the geology and major ore deposits of Central Africa: Explanatory note for the 1:4,000,000 map "Geology and major ore deposits of Central Africa. *J. Afr. Earth Sci.* 44, 571–595. doi: 10.1016/j.jafrearsci.2005.10.016

Murray, J. W., and Dillard, J. G. (1979). The oxidation of cobalt (II) adsorbed on manganese dioxide. *Geochim. Cosmochim. Acta* 43, 781–787. doi: 10.1016/0016-7037(79)90261-8

Nakatsuka, S., Okamura, K., Takeda, S., Nishioka, J., Firdaus, M., Norisuye, K., et al. (2009). Behaviors of dissolved and particulate Co, Ni, Cu, Zn, Cd and Pb during a mesoscale Fe-enrichment experiment (SEEDS II) in the western North Pacific. *Deep-Sea. Res. II.* 56, 2822–2838. doi: 10.1016/j.dsr2.2009.06.008

Parida, K. M., Kanungo, S. B., and Sant, B. R. (1981). Studies on MnO_2-I. chemical composition, microstructure and other characteristics of some synthetic MnO_2 of various crystalline modifications. *Electrochim. Acta* 26, 435–443. doi: 10.1016/0013-4686(81)85033-5

Ren, J. B., He, G. W., Deng, X. G., Deng, X. Z., Yang, Y., Yao, H. Q., et al. (2022). Metallogenesis of Co-rich ferromanganese nodules in the northwestern Pacific: Selective enrichment of metallic elements from seawater. *Ore. Geol. Rev.* 143, 104778. doi: 10.1016/j.oregeorev.2022.104778

Ren, J. B., He, G. W., Yang, Y., Yu, M., Deng, Y. N., Pang, Y. T., et al. (2024). Ultraselective enrichment of trace elements in seawater by Co-rich ferromanganese nodules. *Global Planet. Change* 239, 104498. doi: 10.1016/j.gloplacha.2024.104498

Ren, X. W., Liu, J. H., Cui, Y. C., Shi, X. F., and Yin, J. W. (2011). Effects of phosphatization on enrichment of cobalt in the Co-rich Fe-Mn crusts from seamount MP2 of the Line Islands in the central Pacific. *Adv. Mar. Sci.* 29, 323–329. doi: 10.3969/j.issn.1671-6647.2011.03.008

Ren, X. W., Shi, X. F., Zhu, A. M., Liu, J. H., and Fang, X. S. (2010). Controlling factors on enrichment of cerium in Co-rich Fe-Mn crusts from Magellan Seamount Cluster. *J. Chin. Rare. Earth Soc.* 28 (4), 489–494. Available at: https://www.docin.com/p-1186041205.html (Accessed August 2, 2024).

Takahashi, Y., Manceau, A., Geoffroy, N., Marcus, M. A., and Usui, A. (2007). Chemical and structural control of the partitioning of Co, Ce, and Pb in marine ferromanganese oxides. *Geochim. Cosmochim. Acta* 71, 984–1008. doi: 10.1016/j.gca.2006.11.016

U. S. Geological Survey (2024). "Cobalt," in *Mineral Commodity Summaries 2024* (Washington D.C.: Department of the Interior), 62–63. doi: 10.3133/mineral2024

Xue, T. (2007). *Geochemical characters and ore-forming elements enrichment mechanism of ferromanganese crusts from Pacific Ocean*. Ph.D. dissertation (Guangzhou: Sun Yat-Sen University) (in Chinese with English abstract).